

On the Performance of Dual RIS-assisted V2I Communication under Nakagami- m Fading

Mohd Hamza Naim Shaikh, Khaled Rabie[°], Xingwang Li[#], Theodoros Tsiftsis[†], and Galymzhan Nauryzbayev
School of Engineering and Digital Sciences, Nazarbayev University, Nur-Sultan City, 010000, Kazakhstan

[°]Department of Engineering, Manchester Metropolitan University, Manchester, M15 6BH, UK

[#]School of Physics and Electronic Information Engineering, Henan Polytechnic University, Jiaozuo 454000, China

[†]Department of Informatics & Telecommunications, University of Thessaly, Greece;

[†]School of Intelligent Systems Science and Engineering, Jinan University, China

Email: {hamza.shaikh, galymzhan.nauryzbayev}@nu.edu.kz, °k.rabie@mmu.ac.uk,

[#]lixingwang@hpu.edu.cn, [†]tsiftsis@ieee.org

Abstract—Vehicle-to-everything (V2X) connectivity in 5G-and-beyond communication networks supports the futuristic intelligent transportation system (ITS) by allowing vehicles to intelligently connect with everything. The advent of reconfigurable intelligent surfaces (RISs) has led to realizing the true potential of V2X communication. In this work, we propose a dual RIS-based vehicle-to-infrastructure (V2I) communication scheme. Following that, the performance of the proposed communication scheme is evaluated in terms of deriving the closed-form expressions for outage probability, spectral efficiency and energy efficiency. Finally, the analytical findings are corroborated with simulations which illustrate the superiority of the RIS-assisted vehicular networks.

Keywords— Reconfigurable intelligent surface (RIS), dual RIS, energy efficiency, spectral efficiency, vehicular communication.

I. INTRODUCTION

As a key enabler for intelligent transportation systems (ITSs), vehicle-to-everything (V2X) communication has sparked a renewed interest in the research community. V2X encompasses a wide range of wireless technologies such as vehicle-to-pedestrian (V2P), vehicle-to-infrastructure (V2I), and vehicle-to-vehicle (V2V). Additionally, it also includes the vehicular communications with vulnerable road users (VRUs), grid (V2G), network (V2N) and cloud (V2C) [1]. The V2X communications will be a critical component of the futuristic connected and self-driving cars, envisioned and enabled by the sixth-generation (6G) wireless technologies. Furthermore, the V2X communications will also enhance and transform the quality-of-service (QoS) in terms of unparalleled user experience, ultra-high road safety and air quality improvement. In addition, a slew of advanced applications will also be supported like platooning, trajectory alignments, exchanging sensor data and high precision maps, and so on [2]. Thanks to the enhanced capabilities of 6G, vehicles will receive accurate safety information, intelligent traffic management support, and innovative infotainment features. Thus, the 6G services will be used to create a fully automated, autonomous, and ubiquitously connected vehicular network [3].

Recently, reconfigurable intelligent surfaces (RISs) have emerged as a breakthrough technology that offers a great deal in terms of wireless communication [4]. Inherently, RIS is a

software-defined artificial structure made up of a large number of scattering passive elements, termed as reflecting units (RUs). These RUs are capable to adjust the electromagnetic (EM) properties of a reflected wave that is incident on them. Thus, RIS can use not only this ability to boost the received signal's power, but also the capability to create an additional reflective link to mitigate the impact of blockages. With the large number of RUs, RISs are particularly known to have large spectral and energy efficiency [5]. As a result, RIS may be used to improve the quality of vehicular communication through establishing a low-cost, highly energy efficient indirect line-of-sight (LoS) communications [6].

In [7], the authors investigated the outage performance for RIS-assisted vehicular communication networks. Likewise, the secrecy outage performance of RIS-aided vehicular communications has been studied in [8]. RISs were also investigated for detecting VRUs such as cyclists, pedestrians and wheelchair users [9]. Specifically, the authors utilized RISs for enhancing the radar visibility for VRUs. Further, in [10], the authors provided a optimization framework for resource allocation in the RIS-aided vehicular communications. Specifically, they jointly optimized the power allocation, RIS reflection coefficients and spectrum allocation for different QoS requirements of the V2V and V2I communication links. Likewise, in [11], the authors discussed a system model where RSU leverages RIS to connect the dark zones, i.e., areas blocked due by obstacles. Moreover, a comprehensive overview on the recent advances in 6G vehicular networks was provided in [12, 13], where the authors also described various open challenges and possible research directions.

Motivated by the above, in this work, we investigate the performance of a dual RIS-assisted V2I communication network scenario. Specifically, the proposed scenario considers the uplink transmission where the vehicle is communicating with the base station. To enhance the communication capabilities, the vehicle is supported through two RISs which create a virtual line-of-sight (LoS) link, which, otherwise, was inherently non-LoS (NLoS). The major contributions can be summarized as

- Explicitly, we invoked the central limit theorem (CLT) to characterize the received signal-to-noise ratio (SNR) for

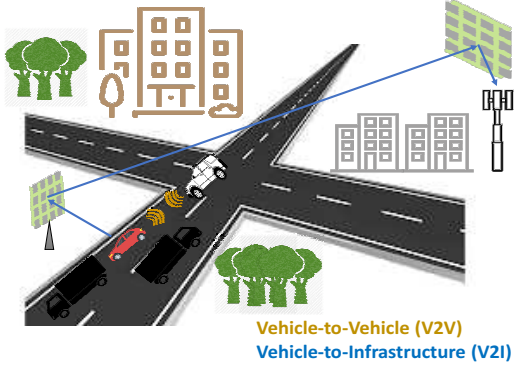


Fig. 1. Schematic for the considered dual RIS-aided V2I communication.

the proposed dual RIS case. Further, based on this, we derived the closed-form expression for outage probability.

- Further, we derived the closed-form expressions for the upper and lower bounds of SE and EE of the proposed dual RIS-assisted V2I communication scenario.
- Finally, as a performance benchmark, the proposed scenario is compared with the single RIS-assisted V2I communication and with RIS V2I communication. The results show the superiority of the proposed scenario of dual RIS-assisted V2I over the single RIS-assisted V2I communication case.

II. SYSTEM MODEL

As illustrated in Fig. 1, in this work, we consider a V2I communication model, wherein the vehicular user (V) tries to communicate with a nearby base station (BS). Apart from the direct cellular link, a reflected path through RISs is considered to support this uplink transmission. In particular, we consider a dual RIS-assisted uplink V2I transmission with two RISs, one each placed near V and BS both, respectively. For the two RISs, the number of RUs is assumed to be M_1 and M_2 for RIS-1 and RIS-2, respectively, while keeping the total number of RUs unchanged, i.e., $M_1 + M_2 = N$, where N is the number of RUs in large RIS for the single RIS scenario, which is the benchmark for comparison. Thus, based on RIS, the following scenarios are considered in this work

- **Dual RIS-assisted Transmission (DRAT):** In DRAT, the transmission takes place only through the two RISs and the reflected link, as shown in Fig. 1.
- **Single RIS-assisted Transmission (SRAT):** In SRAT, the transmission takes place through single large RIS which is placed near to BS.
- **Direct Cellular Transmission (DCT):** In DCT, V communicates with BS directly without utilizing RISs. Thus, the transmission is inherently NLoS and experiences a higher pathloss exponent. This would also serve as the baseline scheme for the performance comparison of the above two cases.

A. Channel Model

The channels between V-to-RIS-1 and RIS-2-to-BS can be modeled as deterministic LOS channels as the distances

are small and the probability of having LoS is very high. However, the distance between RIS-1 and RIS-2 is large and thus the small scale fading for the channel between the i th element of RIS-1 and the j th element of RIS-2, denoted by h_{ij}^{RR} , is modeled through Nakagami- m fading. Hence, for $i = \{1, 2, \dots, M_1\}$ and $j = \{1, 2, \dots, M_2\}$. Further, the distances related to the V-to-RIS-1, RIS-1-to-RIS-2 and RIS-2-to-BS links are represented by d_1 , d_{RR} and d_2 , respectively.

B. Received Signal Model

The received base-band signal at BS, denoted by r , for the dual RIS-aided transmission case can be expressed as

$$r = \sqrt{\mathcal{B} P_t} \left(\sum_{i=1}^{M_1} \sum_{j=1}^{M_2} e^{j\phi_i^{(1)}} h_{ij}^{RR} e^{j\phi_j^{(2)}} \right) s + N_o, \quad (1)$$

where P_t is the transmit power constraint at V, \mathcal{B} is the distance-dependent pathloss, $s \sim \mathcal{CN}(0, 1)$ is the transmitted symbol, and $N_o \sim \mathcal{CN}(0, \sigma^2)$ is the additive white Gaussian noise (AWGN). Further, ϕ_1 and ϕ_2 are the phase of the V-to-RIS1 and RIS2-to-BS channels. Further, for a link distance d , \mathcal{B} at the carrier frequency of 3 GHz can be given by [14]

$$\mathcal{B}(d) [\text{dB}] = \begin{cases} -37.5 - 22 \log_{10}(d/1 \text{ m}) & \text{if LOS,} \\ -35.1 - 36.7 \log_{10}(d/1 \text{ m}) & \text{if NLOS.} \end{cases} \quad (2)$$

Likewise, instantaneous SNR at BS can be formulated as

$$\gamma = \frac{\left| \sum_{i=1}^{M_1} \sum_{j=1}^{M_2} \delta_{ij} e^{j(\phi_i^{(1)} + \phi_j^{(2)} - \varphi_{ij})} \right|^2 \mathcal{B} P_t}{\sigma^2}, \quad (3)$$

where δ_{ij} and φ_{ij} denote the amplitude and phase of h_{ij}^{RR} .

1) **RIS Reflection Parameters:** Now, SNR at BS can be maximized through adjusting the phase at RISs to cancel the resultant phase, i.e., $\phi_i^{(1)} + \phi_j^{(2)} - \varphi_{ij} = 0$, for $i = \{1, 2, \dots, M_1\}$ and $j = \{1, 2, \dots, M_2\}$. Thus, by substituting $\varphi_{ij} = \phi_i^{(1)} + \phi_j^{(2)}, \forall i, j$, the received signal power at BS can be maximized. Consequently, maximized SNR corresponding to the optimal phase can be given as

$$\gamma_{\max} = \frac{\left| \sum_{i=1}^{M_1} \sum_{j=1}^{M_2} \delta_{ij} \right|^2 \mathcal{B} P_t}{\sigma^2} = \frac{A^2 \mathcal{B} P_t}{\sigma^2} = A^2 \mathcal{B} \bar{\gamma}, \quad (4)$$

where $A^2 = \left| \sum_{i=1}^{M_1} \sum_{j=1}^{M_2} \delta_{ij} \right|^2$ is the cascaded channel gain provided by RISs, and $\bar{\gamma} = P_t/\sigma^2$ is transmit SNR.

Likewise, proceeding in the similar way, for the SRAT scenario, maximized SNR at BS can be given as¹

$$\hat{\gamma}_{\max} = \left(\sum_{i=1}^N \beta_i \right)^2 \bar{\gamma} = B^2 \bar{\gamma}, \quad (5)$$

where β_i is the amplitude of a channel between RIS and V, denoted by h_i^{RV} , i.e., $h_i^{RV} = \beta_i e^{-j\varphi_i}$, and B^2 is the corresponding channel gain provided by single RIS.

¹For the SRAT scenario, the analysis is similar. Thus, the detailed description is omitted for the sake of brevity. In particular, for SRAT, large RIS with N RUs is present near BS, where $N = M_1 + M_2$. Likewise, the RIS-to-BS link is also modeled as Nakagami- m fading with the rest of the parameters being the same, as in DRAT, like transmit power constraint at V, etc.

III. PERFORMANCE ANALYSIS

This section initially evaluates SNR for the dual RIS-aided V2I scenario. Utilizing the SNR expressions formulated earlier, the outage probability, SE and EE are derived.

A. Statistical Characterization of the Dual RIS Channel Gain

Now utilizing CLT for $M \gg 1$, $A = \sum_{i=1}^{M_1} \sum_{j=1}^{M_2} \delta_{ij}$ can be approximated through a Gaussian distribution, i.e., $A \sim \mathcal{N}(\mu_A, \sigma_A^2)$ [15], with a probability density function (PDF) given by

$$f_A(y) = \begin{cases} \frac{1}{\sqrt{2\pi\sigma_A^2}} \exp\left(-\frac{(y-\mu_A)^2}{2\sigma_A^2}\right), & \text{if } y > 0, \\ 0, & \text{if } y = 0, \end{cases} \quad (6)$$

where $\mu_A = \sum_{i=1}^{M_1} \sum_{j=1}^{M_2} \mu_{ij}$, $\sigma_A^2 = \sum_{i=1}^{M_1} \sum_{j=1}^{M_2} \sigma_{ij}^2$. Here, μ_{ij} and σ_{ij}^2 are the mean and variance of the random variable δ_{ij} , which follows the Nakagami- m distribution. Hence, $\mu_{ij} = \frac{\Gamma(m_1 + \frac{1}{2})}{\Gamma(m_1)} \sqrt{\left(\frac{\Omega_{m_1}}{m_1}\right)}$ and $\sigma_{ij}^2 = \Omega_{m_1} \left\{1 - \frac{1}{m_1} \left(\frac{\Gamma(m_1 + \frac{1}{2})}{\Gamma(m_1)}\right)^2\right\}$, for all $i = \{1, \dots, M_1\}$ and $j = \{1, \dots, M_2\}$.

Likewise the cumulative distribution function (CDF) of A can be derived from its PDF as

$$F_A(y) = \int_{-\infty}^y f_A(y) dy = \begin{cases} 1 - Q\left(\frac{y-\mu_A}{\sigma_A}\right), & \text{if } y > 0, \\ 0, & \text{if } y = 0. \end{cases} \quad (7)$$

B. Outage Probability

The normalized instantaneous rate, denoted by R_{in} , for the DRAT scenario can be formulated from (4) and expressed as

$$R_{\text{in}} = \log_2(1 + \gamma_{\text{max}}) = \log_2(1 + A^2 \bar{\gamma}). \quad (8)$$

Now, the end-to-end outage from V to BS via RIS, denoted by P_{out} , can be defined in terms of a rate threshold, R_{th} , as

$$\begin{aligned} P_{\text{out}} &= \Pr[R_{\text{in}} < R_{\text{th}}] = \Pr[\log_2(1 + A^2 \bar{\gamma}) < R_{\text{th}}] \\ &= \Pr\left[A < \sqrt{\frac{2^{R_{\text{th}}} - 1}{\bar{\gamma}}}\right] = \Pr[A < \Upsilon_{\text{th}}], \end{aligned} \quad (9)$$

where $\Upsilon_{\text{th}} = \sqrt{\frac{2^{R_{\text{th}}} - 1}{\bar{\gamma}}}$. Thus, the closed-form expression of the outage probability DRAT can be evaluated as

$$\begin{aligned} P_{\text{out}} &= \int_0^{\Upsilon_{\text{th}}} f_A(y) dy, \\ &= F_A(\Upsilon_{\text{th}}) = 1 - Q\left(\frac{\Upsilon_{\text{th}} - \mu_A}{\sigma_A}\right). \end{aligned} \quad (10)$$

C. Spectral Efficiency

SE for the DRAT scenario can be defined from (8) as

$$\begin{aligned} SE &= \mathbb{E}[R_{\text{in}}] = \mathbb{E}[\log_2(1 + A^2 \bar{\gamma})], \\ &= \int_0^{\infty} \log_2(1 + y^2 \bar{\gamma}) f_A(y) dy. \end{aligned} \quad (11)$$

The exact derivation of the integral in (11) is mathematically intractable, and thus a closed-form expression may not be derived. Hence, we resort to approximate SE with tight upper and lower bounds by invoking Jensen's inequality.

1) *Upper Bound*: Applying Jensen's inequality, we define the upper bound for SE as SE_u , where $SE \leq SE_u$. Now, SE_u can be evaluated from (11) as

$$SE_u = \log_2(1 + \bar{\gamma} \mathcal{B} \mathbb{E}[A^2]), \quad (12)$$

and expressed as

$$SE_u = \log_2 \left[1 + \bar{\gamma} \mathcal{B} M_1 M_2 \Omega_{m_1} \times \left\{ 1 + \frac{(M_1 M_2 - 1)}{m_1} \left(\frac{\Gamma(m_1 + \frac{1}{2})}{\Gamma(m_1)} \right)^2 \right\} \right]. \quad (13)$$

Evaluation of Upper Bound: In (12), $\mathbb{E}[A^2]$ can be evaluated utilizing the relation $\text{Var}[X] = \mathbb{E}[X^2] - (\mathbb{E}[X])^2$ as

$$\mathbb{E}[A^2] = \text{Var}[A] + (\mathbb{E}[A])^2 = \sigma_A^2 + \mu_A^2. \quad (14)$$

After substituting the values of μ_A^2 and σ_A^2 in (12), the upper bound for DRAT-based SE can be evaluated.

2) *Lower Bound*: Likewise, we define the lower bound for SE as SE_l , where $SE \geq SE_l$. Now, SE_l can again be defined from (11) as

$$SE_l = \log_2 \left(1 + \frac{\bar{\gamma} \mathcal{B}}{\mathbb{E}\left[\frac{1}{A^2}\right]} \right), \quad (15)$$

and expressed as given in (16), on the top of next page.

Evaluation of Lower Bound: In (15), the expectation $\mathbb{E}\left[\frac{1}{A^2}\right]$ can be solved utilizing the Taylor series expansion and approximated as [15]

$$\mathbb{E}\left[\frac{1}{A^2}\right] \approx \frac{1}{\mathbb{E}[A^2]} + \frac{\text{Var}[A^2]}{[\mathbb{E}[A^2]]^3}. \quad (17)$$

Since the statistical characteristics of A is known to be Gaussian distributed (as discussed earlier in subsection A), A^2 will follow a non-central chi-square distribution. Thus, the mean and variance of A^2 can be expressed as

$$\text{Var}[A^2] = 2\sigma_A^2 (\sigma_A^2 + 2\mu_A^2), \quad (18)$$

$$\mathbb{E}[A^2] = \sigma_A^2 + \mu_A^2, \quad (19)$$

respectively. Thus, utilizing these expressions and substituting the values of μ_A^2 and σ_A^2 , the lower bound for SE of the DRAT scenario can be evaluated.

3) *Approximation for Large M*: We define \overline{SE} as approximate SE (ASE) for large M_1 and M_2 . Now, with the upper and lower bounds of SE of the DRAT scenario, exact SE lies in-between and can be expressed as

$$SE_l \leq SE \leq SE_u. \quad (20)$$

However, for larger M_1 and M_2 , i.e., $M_1, M_2 \gg 1$, both SE_l and SE_u converge to \overline{SE} . Thus, ASE can be given as

$$\overline{SE} = \log_2 \left[1 + \bar{\gamma} \mathcal{B} \frac{M_1^2 M_2^2 \Omega_{m_1}}{m_1} \left(\frac{\Gamma(m_1 + \frac{1}{2})}{\Gamma(m_1)} \right)^2 \right]. \quad (21)$$

It can be noted from (21) that, through utilizing dual RIS, the fourth order channel gain can be realized, i.e., $M_1^2 M_2^2$, whereas, for single RIS, the maximum channel gain is of the second order, i.e., N^2 .

$$SE_l = \log_2 \left[1 + \bar{\gamma} \mathcal{B} \frac{M_1 M_2 \Omega_{m_1} \left\{ 1 + \frac{(M_1 M_2 - 1)}{m_1} \left(\frac{\Gamma(m_1 + \frac{1}{2})}{\Gamma(m_1)} \right)^2 \right\}^3}{2 \left\{ 1 + \frac{(2M_1 M_2 - 1)}{m_1} \left(\frac{\Gamma(m_1 + \frac{1}{2})}{\Gamma(m_1)} \right)^2 \right\} \left\{ 1 - \frac{1}{m_1} \left(\frac{\Gamma(m_1 + \frac{1}{2})}{\Gamma(m_1)} \right)^2 \right\} + \left\{ 1 + \frac{(M_1 M_2 - 1)}{m_1} \left(\frac{\Gamma(m_1 + \frac{1}{2})}{\Gamma(m_1)} \right)^2 \right\}^2} \right] \quad (16)$$

TABLE I
SIMULATION PARAMETERS

Parameter	Simulation Values
Circuit Power	$P_{BS}=10$ dBm, $P_U=10$ dBm [5]
Fading Parameter for DRAT	$m_1=10$
Fading Parameter for Direct Links	$m_3=1$
RIS Power Consumption	$P_{RE}=10$ dBm [5]
HPA Power Consumption Factor	$\alpha=1.2$
Noise Floor	$\sigma^2=-120$ dBm

D. Energy Efficiency

Now, EE of the dual RIS-aided system is defined as the ratio of SE over the total power consumed and can be expressed as $EE = \frac{SE}{P_{tot}}$, where P_{tot} denotes the total power consumed, which consists of the transmit power, the circuit power consumption at BS and V, and the power consumed at RIS. Considering all the power consumed, the EE in can be expressed

$$EE = \frac{SE}{(1 + \xi)P_t + P_V^c + (M_1 + M_2)P_{RIS}^c + P_{BS}^c}, \quad (22)$$

where P_{RIS}^c denotes the power utilized by each RU, $\xi = \frac{1}{\omega}$ and ω is the drain efficiency of HPA. Likewise, P_V^c , i.e., the power consumed in other circuit components excluding HPA at V and P_{BS}^c is the circuit power consumption at BS.

This completes the analytical derivation of the outage, SE, and EE for DRAT of the uplink of V2I communication.

IV. SIMULATION RESULTS

This section discusses and presents the simulation results for the performance of the dual RIS-assisted V2I communication. Further, the results for the SRAT and DCT scenarios are presented for the sake of comparison. The distances between V-to-RIS1, RIS1-to-RIS2 and RIS2-to-BS are assumed to be 5, 100 and 5 meters, respectively. Similarly for the simulation purpose, $M = M_1 = M_2$ and N is taken as to be $N = 2M$, in order to maintain the fairness in the comparison. The rest of the simulation parameters are summarized in Table I.

Fig. 2 shows the SE performance for the DRAT scenario, where the solid lines without marker points show the exact (simulation) performance of DRAT, whereas the markers show the analytically derived upper and lower bounds on SE. Additionally, ASE for large M is also plotted. The simulation verifies that the derived upper and lower bounds are quite tight as the analytically derived bounds are remarkably close to the actual performance. Further, it can also be noted that the difference between exact SE and ASE (as shown in (21)) diminishes as M increases. For instance, at $M = 10$ and

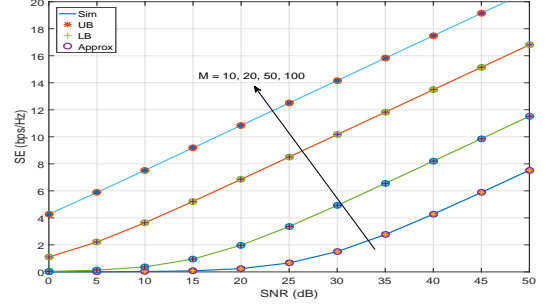


Fig. 2. SE with respect to $\bar{\gamma}$ for different M of the proposed DRAT scenario.

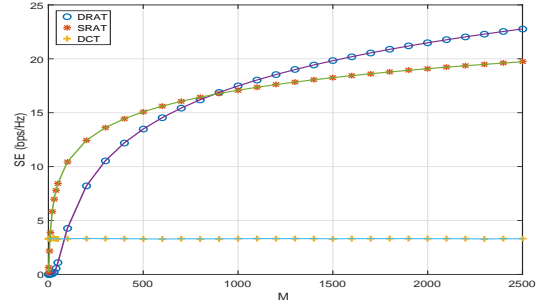


Fig. 3. SE with respect to M for the proposed DRAT scenario.

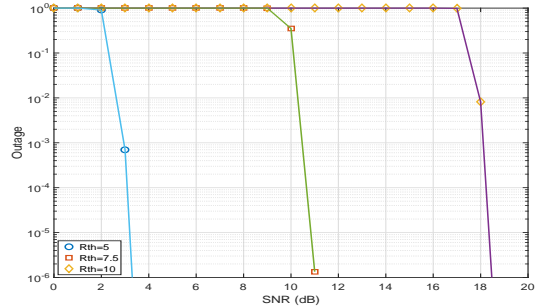
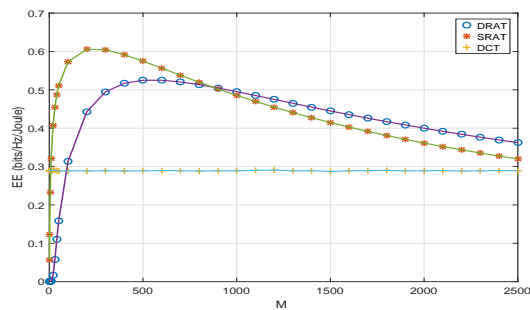


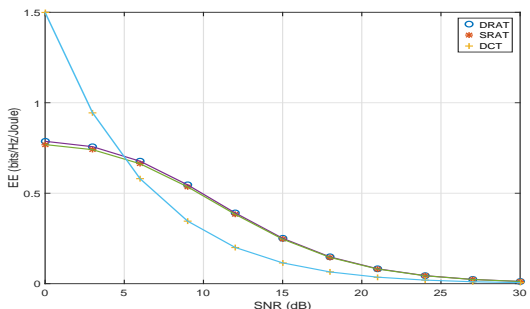
Fig. 4. Outage with respect to P_t for different rate thresholds for DRAT.

$\bar{\gamma} = 30$ dB, SE is 1.5037 bps/Hz whereas \overline{SE} is 1.5034 bps/Hz; however, at $M = 50$ and $\bar{\gamma} = 15$ dB, SE is 5.2201 bps/Hz whereas \overline{SE} is 5.2200 bps/Hz. Thus, it shows that the bounds are quite accurate and near to the exact simulation value.

Fig. 3 shows the SE results for the DRAT scenario, and compares them with the SRAT and DCT scenarios. Specifically, it shows SE for a varying number of RUs. The following observations can be easily inferred from this plot: 1) Apart from smaller M , SE of DRAT is always better than SE of the SRAT scheme due to the fourth order gain provided by dual RIS. This can also be inferred from the analytical evaluation in (31). 2) Due to the multiplicative pathloss, for less number of RUs, i.e., smaller M , the DCT scenario may provide better SE performance than the RIS-reflected link for both DRAT and



(a) EE with respect to M , here $P_t = 10$ dBm.



(b) EE with respect to SNR, here $M = 1000$.

Fig. 5. EE comparison for DRAT with respect to the SRAT and DCT scenarios.

SRAT scenarios. However, as the number of RUs increases, the RIS-based scenarios outperform DCT. 3) Similar to single RIS, dual RIS-based DRAT also suffers from the multiplicative effect of pathloss. Thus, for smaller RUs, the SRAT scenario shows better SE than the DRAT one. 4) As the number of RUs increases sufficiently, DRAT outperforms SRAT significantly.

Fig. 4 shows the outage probability of the DRAT scenario for three different rate thresholds, i.e., $R_{th} = \{5, 7.5, 10\}$ bps/Hz. As evident from the result, the outage can be improved either through increasing the transmit power or the number of RUs. Since, the transmit power at BS is usually constrained, RIS provides an alternate to improve the outage through increasing RUs, instead of increasing the transmit power. Thus, to circumvent the power constraint, the number of RUs at RIS can be scaled accordingly.

Fig. 5 shows the EE results of the DRAT scenario, the EE plots of the SRAT and DCT scenarios are also plotted here for comparison. Specifically, in Fig. 5(a), the performance is with respect to M , while in Fig. 5(b), the EE curve is plotted against SNR. It can be observed that, for large M , the DRAT scenario is the most energy-efficient. Although, for smaller M , single RIS provides better EE; this is due to the fact that the received signal of the dual RIS-reflected link suffers from the multiplicative pathloss that can be mitigated by by large M .

From the above results on SE and EE, it can be easily inferred that the proposed DRAT scheme outperforms SRAT in terms of both SE as well as EE. Similarly, the above results also show that, for a fixed rate requirement, DRAT requires lower transmit power and hence is more energy efficient.

V. CONCLUSION

V2X has opened up a slew of novel possibilities in the wireless vehicular communication arena, but its potential for enabling true ITS has yet to be explored completely, despite its significant importance in the safety of autonomous driving. In this work, we have envisioned the integration of RIS into vehicular networks to realize the true potential in enhancing the performance of the V2I communication. Specifically, we have evaluated the performance of a dual-RIS assisted V2I uplink communication scenario in terms of the outage probability, SE and EE. Novel closed-form expressions are derived and verified through the extensive numerical simulations. The results show a significant gain in the performance can be achieved through the proposed RIS scenario.

VI. ACKNOWLEDGEMENT

This work was supported by the Nazarbayev University CRP Grant no. 11022021CRP1513.

REFERENCES

- [1] J. Wang, K. Zhu, and E. Hossain, "Green internet of vehicles (IoV) in the 6G era: Toward sustainable vehicular communications and networking," *IEEE Trans. Green Commun. Netw.*, vol. 6, no. 1, pp. 391–423, Mar. 2022.
- [2] Y. Cao, S. Xu, J. Liu, and N. Kato, "Toward smart and secure V2X communication in 5G and beyond: A UAV-enabled aerial intelligent reflecting surface solution," *IEEE Veh. Tech. Mag.*, 2022.
- [3] X. Cheng, Z. Huang, and S. Chen, "Vehicular communication channel measurement, modelling, and application for beyond 5G and 6G," *IET Commun.*, vol. 14, no. 19, pp. 3303–3311, 2020.
- [4] Q. Wu, S. Zhang, B. Zheng, C. You, and R. Zhang, "Intelligent reflecting surface-aided wireless communications: A tutorial," *IEEE Trans. Commun.*, vol. 69, no. 5, pp. 3313–3351, May 2021.
- [5] C. Huang, A. Zappone, G. C. Alexandropoulos, M. Debbah, and C. Yuen, "Reconfigurable intelligent surfaces for energy efficiency in wireless communication," *IEEE Trans. Wireless Commun.*, vol. 18, no. 8, pp. 4157–4170, Aug. 2019.
- [6] M. A. Javed *et al.*, "Reliable communications for cybertwin driven 6G IoVs using intelligent reflecting surfaces," *IEEE Trans. Ind. Info.*, 2022.
- [7] J. Wang *et al.*, "Outage analysis for intelligent reflecting surface assisted vehicular communication networks," in *IEEE Global Commun. Conf.*, 2020, pp. 1–6.
- [8] Y. Ai *et al.*, "Secure vehicular communications through reconfigurable intelligent surfaces," *IEEE Trans. Veh. Tech.*, vol. 70, no. 7, pp. 7272–7276, Jul. 2021.
- [9] S. K. Dehkordi and G. Caire, "Reconfigurable propagation environment for enhancing vulnerable road users' visibility to automotive radar," in *IEEE Intelligent Veh. Symp. (IV)*, 2021, pp. 1523–1528.
- [10] Y. Chen *et al.*, "Resource allocation for intelligent reflecting surface aided vehicular communications," *IEEE Trans. Veh. Tech.*, vol. 69, no. 10, pp. 12 321–12 326, Oct. 2020.
- [11] A. Al-Hilo *et al.*, "Reconfigurable intelligent surface enabled vehicular communication: Joint user scheduling and passive beamforming," *IEEE Trans. Veh. Tech.*, vol. 71, no. 3, pp. 2333–2345, Mar. 2022.
- [12] M. Noor-A-Rahim *et al.*, "6G for vehicle-to-everything (V2X) communications: Enabling technologies, challenges, and opportunities," 2020. [Online]. Available: <https://arxiv.org/abs/2012.07753>
- [13] Y. Zhu *et al.*, "Intelligent reflecting surface-aided vehicular networks toward 6G: Vision, proposal, and future directions," *IEEE Veh. Tech. Mag.*, vol. 16, no. 4, pp. 48–56, Dec. 2021.
- [14] E. Bjornson, O. Ozdogan, and E. G. Larsson, "Intelligent reflecting surface versus decode-and-forward: How large surfaces are needed to beat relaying?" *IEEE Wireless Commun. Lett.*, vol. 9, no. 2, pp. 244–248, 2020.
- [15] D. Kudathanthirige, D. Gunasinghe, and G. Amarasingha, "Performance analysis of intelligent reflective surfaces for wireless communication," in *IEEE Int. Conf. Commun. (ICC)*, 2020, pp. 1–6.